

Self-Tuning, Load-Mitigating Feedback Control of a 3-DOF Point Absorber

Dominic D. Forbush, Giorgio Bacelli, Ryan G. Coe

Abstract—A simple, self-tuning multi-objective controller is demonstrated in simulation for a 3-DOF (surge, heave, pitch) point absorber. In previous work, the proposed control architecture has been shown to be effective in experiments for a variety of device archetypes for the single objective of the maximization of electrical power capture: here this architecture is extended to reduce device loading as well. In particular, PTO actuation forces and the minimization of fatigue damage (determined from the sum of wave-exerted and PTO forces) are considered as additional objectives for the self-tuning controller. Because the electrical power surface is consistently fairly flat in the vicinity of control parameters that maximize power capture in contrasting sea-states (i.e., WECs are often broad banded), it is found to be generally possible to mitigate either fatigue damage or PTO load. However, PTO load is found to contradict with fatigue damage in some sea-states, limiting the efficacy of control objectives that attempt to mitigate both simultaneously. Additionally, coupling between the surge and pitch DOFs also limits the extent to which fatigue damage can be mitigated for both DOFs in some sea-states. Because control objectives can be considered a function of the sea-state (e.g., load mitigation may not be a concern until the sea is sufficiently large) a simple transition strategy is proposed and demonstrated. This transition strategy is found to be effective with some caveats: firstly, it cannot circumvent the aforementioned objective contradictions. Secondly, the thresholds at which objective transitions occur are somewhat exceeded: in this respect they cannot be considered as constraints and must be selected more conservatively. Finally, selection of well-performing transition parameters can be a function of sea-state. While a simple selection procedure is proposed, it is non-optimal, and a more robust selection procedure is suggested for future work.

Index Terms—wave energy, linear control, adaptive control, spectral analysis, multi-objective control

Manuscript submitted 10 May, accepted 28 Oct 2021, revised 2 February, published 10 June 2022. This is an open access article distributed under the terms of the Creative Commons Attribution 4.0 licence (CC BY <http://creativecommons.org/licenses/by/4.0/>). unrestricted use (including commercial), distribution and reproduction is permitted provided that credit is given to the original author(s) of the work, including a URI or hyperlink to the work, this public license and a copyright notice.

This work was funded by the Water Power Technologies Office of the United States Department of Energy. Sandia National Laboratories is a multimission laboratory managed and operated by National Technology and Engineering Solutions of Sandia, LLC, a wholly owned subsidiary of Honeywell International Inc., for the U.S. Department of Energy's National Nuclear Security Administration under contract DE-NA0003525. This paper describes objective technical results and analysis. Any subjective views or opinions that might be expressed in the paper do not necessarily represent the views of the U.S. Department of Energy or the United States Government. This article has been subject to single-blind peer review by a minimum of two reviewers.

D. Forbush, G. Bacelli and R. Coe are at Sandia National Labs., Albuquerque, NM 87123 USA (e-mail dforbus@sandia.gov).

Digital Object Identifier <https://doi.org/10.36688/imej.5.23-35>

I. INTRODUCTION

Ocean waves are an energy-dense form of renewable energy. Numerous wave energy converter (WEC) technologies have been proposed to harvest this resource, but substantial technical hurdles continue to prevent this form of energy from being economically viable for grid-scale energy generation. Effective WEC control can significantly enhance power capture and reduce overall cost of energy [1] [2], particularly when coupled with a well-designed power-take-off (PTO) [3]. Theoretically optimal “complex-conjugate” control of a WEC requires advanced knowledge of the affecting wave [4], but can maximize the mechanical power capture of a WEC. Relevant research frequently focuses on accurate future-state wave prediction and prediction-based WEC control strategies to obtain this advance knowledge [5], [6], [7], [8]. This architecture adds complexity to implementation: the prediction is needed in real-time, which requires either a displaced or remote measurement of incoming waves and an accurate model of wave propagation, or a state-estimation procedure that can be computationally intensive. Alternatively, approximations of theoretically optimal control that do not require prediction of future waves, but a frequency-domain estimate of the current sea-state have been pursued [9], [3], [10]. These control strategies can capture > 90% of the energy of a theoretically optimal controller [11], while relying upon a relatively simpler implementation. Regardless of architecture, a successful controller will optimize WEC performance over the changing sea-states to which the device will be subjected. This implies that a control law relying on a spectral estimate of the sea-state must update this estimate over time, and simple estimation procedures relying on identified linear system models have been demonstrated in [10].

Often, the performance of a controller is measured in terms of power capture. However, it is broadly accepted that the consumer cost of energy generated by WEC devices is also a strong function of their durability and overall longevity at sea [12]. To this end, both devices and controllers have been developed with load mitigating properties intended to increase survivability. An example of the former are flap-type oscillating surge devices, which, by nature of their geometry, reduce excitation in larger waves by decreasing WEC area near the energetic free surface [13]. An example of the latter is the inclusion of constraints in model-predictive control laws that predict and regulate the extent of travel and magnitude of force exerted by the dynamic bodies of a WEC in the presence of

extreme waves [14].

The present work expands upon [10], which proposed simple self-tuning linear feedback control law that adjusts the motor torques to maximize electrical power capture and examined it in laboratory experiments of a three degree-of-freedom point absorber in changing sea-states. Here, the controller objective is expanded to include a reduction in PTO-exerted forces and the minimization of fatigue damage. The expanded formulation is examined in simulation. The control law uses a spectral estimation of the wave excitation forces that relies on an identified model of device intrinsic impedance and selection of objective weights describing the relative importance of control objectives. Additionally, a transition strategy is proposed that automatically adjusts control priorities as sea-states become more (or less) energetic based upon user-defined thresholds. The performance of the control law is considered by comparing the loads and power captures of the power-maximizing single-objective controller and the multi-objective load mitigating controllers in contrasting and time-varying sea-states.

II. METHODS

The control approach is first described in detail, along with the device to be simulated. The simulation is subsequently discussed

A. Intrinsic Impedance

The control law relies fundamentally on an linear model of the device intrinsic impedance. The model identification procedure is an application of methods proposed in [15] and is briefly summarized here, with a detailed examination in [16]. In this application, intrinsic impedance, Z_i , describes the relationship between input velocity to output force/torque in the frequency domain, or

$$\begin{aligned} Z_i V(\omega) &= F_{tot}(\omega) \\ \{Z_i, V\} &\in \mathbb{C}^n; n > 1 \end{aligned} \quad (1)$$

where V is the velocity in each degree of freedom (DOF), F_{tot} is the total force applied to the DOF, and ω is the radian frequency. Z_i , V , and F_{tot} are all complex numbers of n DOFs. Generally, all terms (except ω) are 6-element vectors, with each element corresponding to a DOF. A system with reduced DOF can be modeled by either zeroing restrained DOFs or reducing the dimensions of each term. An estimate of Z_i is usually available early in the design process, as it can be computed from a boundary element method (BEM) procedure once a hull geometry and kinematics are defined. Following from the frequency-domain equation of WEC motion

$$\begin{aligned} [i\omega(M + m(\omega)) + B_v + R(\omega) + \frac{S}{i\omega}]V(\omega) \\ = F_e(\omega) + F_{PTO}(\omega) \end{aligned} \quad (2)$$

where F_e is the excitation force exerted by the wave, F_{PTO} is the power-take-off force, m is the added mass,

R is the radiation damping, V is device velocity, M is static inertia B_v captures additional viscous damping, and the hydrostatic stiffness matrix is S . Terms can be rearranged to form the ratio in Eq. 1

$$Z_{BEM}(\omega) = i\omega(M + m(\omega)) + B_v + R(\omega) + \frac{S}{i\omega}. \quad (3)$$

This is an early-stage estimate of Z_i that is useful to design, though it has known limitations [17]. BEM codes assume small-amplitude motions and rely on potential flow theory which assumes viscosity $B_v = 0$. Additionally, as-built devices have more complex dynamics like viscous drag, non-ideal power-take-offs, and mooring dynamics which may not be exactly quantifiable prior to deployment, and may cause actual Z_i to deviate significantly from BEM estimates. A more robust estimate of device impedance can be determined by following the methods of [18], utilized in [19], directly on velocity and force data from physical or numerical experiments which can be conducted on either full or model-scale devices.

A derivation from experimental data effectively linearizes actual device dynamics in the identification of linear models. A schematic of the test procedure used to identify device impedance from experimental results is given as Figure 1. First, in an acquiescent wave tank or calm sea, uncorrelated band-limited (constrained to the frequency range of interest, in this case 0 to 2 Hz) white noise signals are used to excite the device in all three DOF at the PTOs. This test is repeated a minimum of two times, with distinct phase realizations for each repetition. This allows the device intrinsic impedance to be calculated from the three independent experiments: one experiment for each unique set of phase realizations of the excitation signals. Secondly, this procedure is repeated with pink waves in the basin. Using the intrinsic impedance $Z_i(\omega)$ model just calculated, the measured device dynamics resulting from controller actuation can be subtracted, with the difference representing device motion due to wave excitation.

$$F_e(\omega) = Z_i(\omega)V(\omega) - F_{PTO}(\omega) \quad (4)$$

From this difference, a wave excitation model $H(\omega)$ of the physical device as seen at the PTO can be determined (Figure 1), given knowledge or measurement of the exciting wave spectra $\eta(\omega)$. This is particularly useful for multiple-body devices, where BEM estimates of $H(\omega)$ may not reflect excitation dynamics at the PTO, which are of interest here. This procedure is detailed in [18]. A model of $H(\omega)$ is not needed to derive or apply this controller, only an estimate of F_e (Eq. 4). However, $H(\omega)$ is convenient in numerical experiments to convert a prescribed sea-state spectra to an excitation spectra.

In the forthcoming simulations, the simulated model does introduce BEM-excluded quantities that affect the impedance of the simulated device. While these quantities must be specified for deterministic simulation, it is emphasized that the system identification procedure does not use knowledge of these quantities, relying

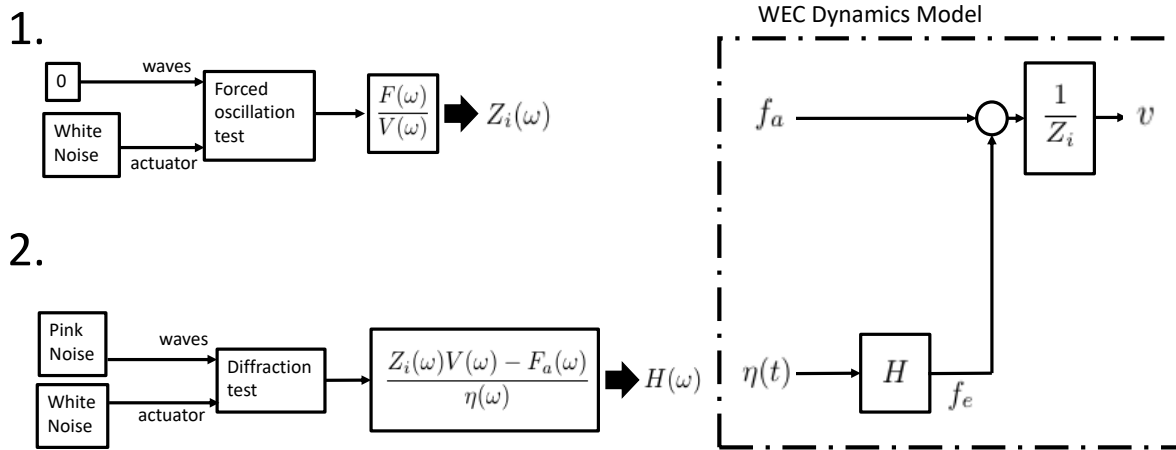


Fig. 1: System identification workflow used for WaveBot (adapted from [16]).

only on simulation outputs of force and velocity to estimate Z_i as per Eq. 1. In this way, it is a plausible representation of the work-flow of a realistic WEC deployment.

B. WaveBot Device

The WaveBot is a single-body three DOF point-absorber style device with independent actuators in heave, surge, and pitch. It was tested in the Naval Surface Warfare Center at Carderock Maneuvering and Sea-keeping Basin in experimental campaigns detailed in [20] and [19], where the device and test facility are also thoroughly described. It is held from an above-water support suspended from a bridge traversing the wave basin (Figure 2). It has an outer radius of 0.88 m, a bottom radius of 0.35 m, and an overall height from the flat bottom to the top of edge of the cylindrical surface of the device is 0.73 m. In calm water, the free-surface of the device is 0.53 m above the flat bottom. In lieu of a mooring, a spring of 24 kN/m provides a restoring force in surge, and the tower prevents motion in the non-actuated degrees of freedom (sway, roll, and yaw). From these tests, linear models of the WaveBot device impedance and excitation were identified and found to be accurate and robust for the sea-states considered herein (Figure 3).

During these physical tests, a self-tuning controller that optimized the capture of electrical power was demonstrated in real-time with 1 KHz sampling [10]. The real-time computed gains closely coincide with optimal gains post-calculated via brute-force, and even for an imperfect estimate of excitation spectra and device impedance, the resulting power captures are nearly identical. The speed and success of the optimization scheme can be attributed to the convexity of the electrical power surface as a function of control gains. The tolerance to modeling error is because the electrical power capture is relatively insensitive to gain selection in the vicinity of optimal values. Thus, the objective surface in this case is very well-suited to a simple optimization scheme of sufficient speed to be run in real-time at 1 KHz sampling rates.

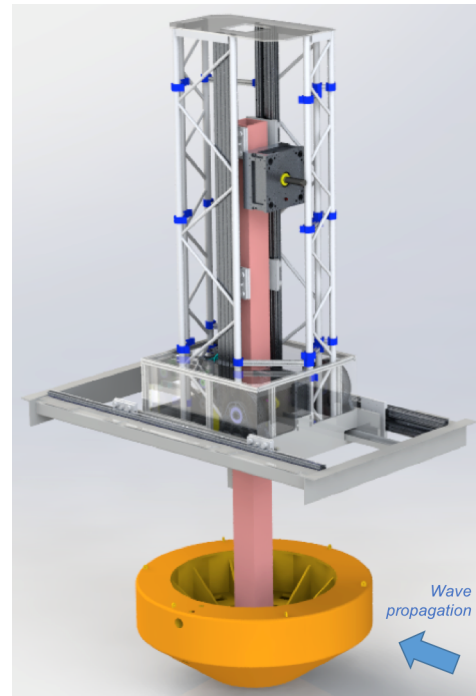


Fig. 2: A rendering of the WaveBot device.

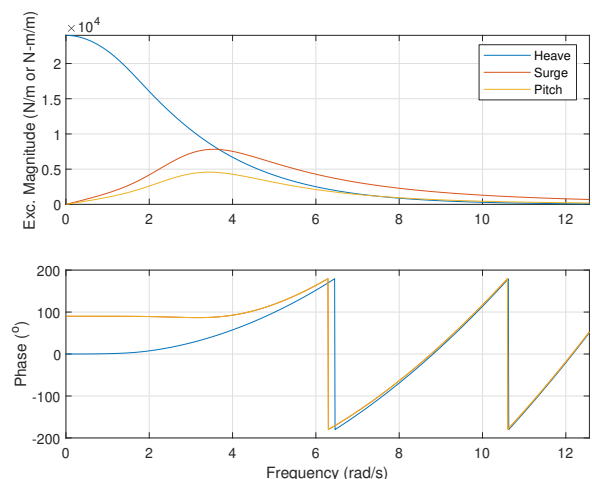


Fig. 3: The surge, heave, and pitch excitation of the WaveBot device.

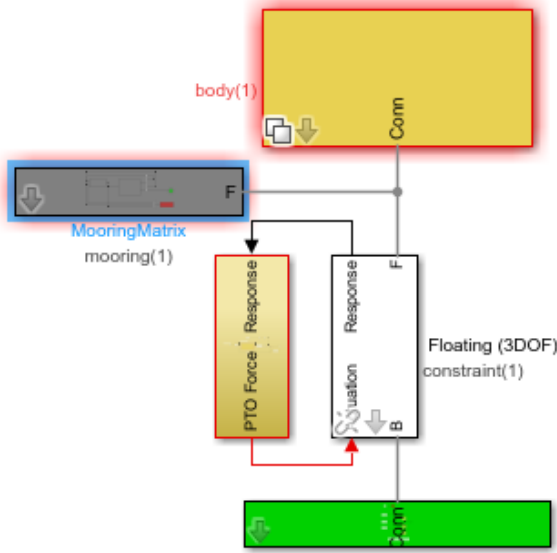


Fig. 4: The top level of the WEC-Sim model of the WaveBot device. The surge restoring spring is included as the mooring block, and the floating (3DOF) constraint applies the controller actuation to the body as prescribed by the PTO Force output, based upon measurements of the device response.

This device and control scheme were recreated in a Wave Energy Converter Simulator (WEC-Sim) model (Figure 4). WEC-Sim uses the time-domain Cummins equation to model WEC motion in the MATLAB Simulink environment, informed by BEM hydrodynamic coefficients [21]. Simulation in this way allows modeling of dynamic constituents not captured by BEM, like viscous drag, along with mooring dynamics. The parameters employed in this study are tabulated in Table I. Within WEC-Sim, quadratic form drag is specified via

$$F_{drag} = \frac{1}{2} \rho A C_d v^2 \quad (5)$$

where ρ is the fluid density (1025 kg/m³), and v (m/s, rad/s) is the linear or angular (as appropriate) velocity vector of the device. Characteristic drag area A (m²) and drag coefficient C_d are user-specified parameters.

Aside from system identification efforts, which do not use exciting waves, two distinct sea-states, described as idealized unidirectional JONSWAP spectra ($\gamma = 3.3$) were evaluated [22]. Sea-state 2 has a model period of 1.6 s and a model significant wave height of 0.127 m. Sea-state 10 has a model period of 3.5 s and a model significant wave height of 0.254 m (Figure 5). For brevity, only results from sea-state 10 are presented in detail, but all sea-states are discussed.

C. Spectral Estimations

The controller and objective functions utilize frequency-domain estimations of various parameters. For solver stability, the simulation time step was 0.01 s. For this study, frequency domain estimations were performed over 256 second windows of the concerned,

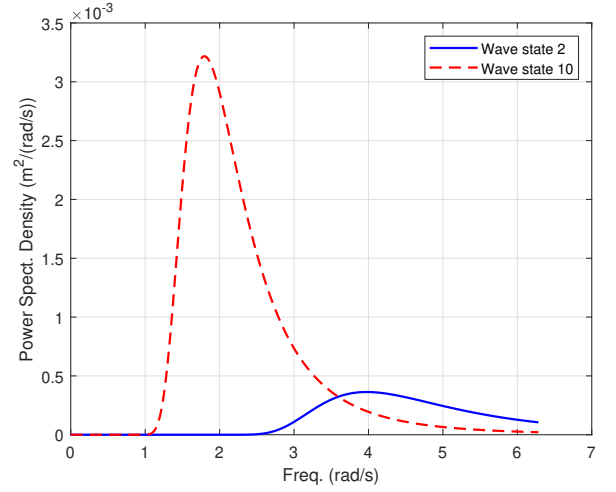


Fig. 5: Nominal power spectral density of the contrasting sea-states for which the controller was evaluated.

de-trended quantities, with successive windows overlapping by 255 seconds. The 100 Hz data is first down-sampled to 4 Hz, such that the Nyquist frequency of the resulting estimate 2 Hz, sufficiently high to resolve all relevant dynamics for the examined sea-states. This buffer was then down-sampled again, such that subsequent calculations used a buffer updated every 8 seconds of simulated time. A Hamming window of equal length is applied to the data buffer, and then the discrete Fourier Transform is applied. Data buffers were initialized with zeros. This implies that at the start of each simulation, any spectral estimation procedure requires a minimum of 256 s to accurately reflect spectral amplitude. Although the repeat time of an irregular wave is known explicitly in simulation, it is not realistic to presume this knowledge. Because windows are not likely to capture integral numbers of data periods, some variation window-to-window frequency domain estimates are expected even in statistically stationary conditions.

This procedure was utilized here to align with the approach taken in experiment [19]. Controller adjustment times can be shortened by using a shorter window, but at the expense of decreased frequency resolution, but 256 s is retained in this application as it is sufficiently short to allow controller parameters to adapt to sea-states changing on realistic time-scales. Changes in frequency content resulting from updated control parameters, which update (practically) instantaneously will also be delayed as a result of the necessary windowing. The maximum functional rate at which control parameters can be changed is limited by this innate delay.

D. Feedback Control

The mechanical power absorbed by a WEC over the whole frequency range is defined by integration

$$W_{PTO} = \frac{1}{2\pi} \int_0^{\infty} [F_{PTO}(\omega)V^*(\omega) + F_{PTO}^*(\omega)V(\omega)]d\omega \quad (6)$$

TABLE I: WEC-Sim parameters for system identification and control simulations

Parameter	Surge	Heave	Pitch
Linear Damping (N/s, N-m/s)	1000	1000	100
Mooring Damping (N/s, N-m/s)	5	5	0
Quadratic Drag $C_d A$ (m ²)	3.40	5.74	2.74
Mooring Stiffness (N/m, N-m/rad)	24000	5000	3000

where $*$ denotes the complex conjugate. It can be shown [23] that W_{PTO} is minimized (by sign convention, this maximizes power capture) when

$$F_{PTO}(\omega) = Z_i^*(\omega)v(\omega) \quad (7)$$

demonstrating that device intrinsic impedance is innate in maximization of mechanical power. This is the reason complex conjugate control is regarded as the theoretically optimal controller.

However, this is difficult to actualize in practice because the complex conjugate Z_i^* is noncausal [23]. This implies that an advance measurement or model of incoming waves and a wave propagation model is necessary to implement this controller, both of which can be confounded in short-crested seas [24]. Further, maximization of mechanical power does not imply a maximization of useful power, as often the generation of electrical energy is the objective of a WEC and the efficient operation of the power conversion chain rarely implies operating conditions conducive to mechanical power optimization [25] [19].

It has been shown that simple feedback controllers can approximate complex conjugate controllers over finite frequency bands [26] [27]. Because realistic sea-states are generally band-limited [11], these controllers can offer commensurate performance at substantially reduced implementation complexity. For this application, we focus on the widely familiar proportional-integral control law, where a PTO force is described based upon a measurement of device velocity

$$F_{PTO}(s) = \frac{(K_P s + K_I)}{s} V(s) \quad (8)$$

where s denotes the Laplace transform variable, and K_P and K_I are the proportional and integral control gain matrices it is our objective to optimally determine. For the objective of power maximization, the abstraction of impedance is again useful by recognizing that

$$Z_{PTO}(s) = \frac{K_P s + K_I}{s} \quad (9)$$

from which the optimal gains for a complex conjugate controller follow immediately from Eq. 7 and 3 for a single frequency [26]. Because realistic seas are narrow-banded, the approximation of optimal complex conjugate control at a single frequency results in a high fractional power capture [11], though the ideal single frequency at which power capture is maximized does not share the closed-form solution of the monochromatic case and is instead determined via optimization. For this controller to optimize electrical power, it is necessary to consider the specifics of the power conversion chain as well.

The total electrical power delivered by the WEC is

TABLE II: PTO Parameters

Parameter	Surge	Heave	Pitch
R (Ohm)	0.50	0.50	0.50
N	12.46	12.46	3.00
K_t (N-m/Amp)	6.17	6.17	6.17

$$P_{abs} = \mathcal{R}((NK_t)^{-1}C\Omega)^*((K_e N + R(NK_t)^{-1}C)\Omega) \quad (10)$$

where \mathcal{R} takes the real part, R is the phase-to-neutral resistance of the motor (Ohm), N is the gear ratio between the wave-interacting body and the PTO in that DOF, K_t is the motor torque constant (N-m/Amp), K_e is the motor back-EMF constant (rad/(V-s)), estimated as $\frac{2}{3}K_t$, and

$$\Omega = (Z_i - C)^{-1}F_e \quad (11)$$

where C is the control matrix. Excitation force F_e is estimated using the identified model Z_i by the method outlined in [10]. For brevity, this method will not be reiterated here, but it is emphasized that this estimate is obtained without the use of external wave sensors or propagation models. PTO parameters are summarized in Table II.

For the diagonal PI controller selected for this investigation

$$C = \begin{bmatrix} K_p^h + \frac{K_i^h}{s} & 0 & 0 \\ 0 & K_p^s + \frac{K_i^s}{s} & 0 \\ 0 & 0 & K_p^p + \frac{K_i^p}{s} \end{bmatrix} \quad (12)$$

By the controller sign convention established in Eq. 8, power is usefully extracted by the WEC when $P_{abs} < 0$. For a given excitation force spectra F_e and device intrinsic impedance model Z_i , the optimal set of controller gains

$$\eta_{opt} = \{K_p^h, K_i^h, K_p^s, K_i^s, K_p^p, K_i^p\}$$

to maximize electrical power is the result of the optimization

$$\eta_{opt} = \arg \min P_{abs}(\eta, F_e) \quad (13)$$

E. Expanding to Multiple Objectives

Thus far, only power maximizing (mechanical and electrical) objectives have been considered. However, it has been well-established that mitigating structural and power train loads are important to device survival and longevity, and can contribute to reductions in cost-of-energy by decreasing maintenance need and increasing up-time [12] [28] [29]. Because PTO electrical

and mechanical components must be sized to based upon anticipated loads, reducing PTO loads can reduce device cost. To minimize the levelized cost of energy of a device an ideal controller must be multi-objective by balancing mitigation of loads with the maximization of power. The previous success of the optimization scheme for power-maximization objectives relied upon the amenable traits of the objective surface [10]: for such an optimizer to retain its utility for a more involved cost function, it is desirable that the objective surface retain its convexity and small gradients in the vicinity of the optimum.

To expand the cost function, first consider the loads exerted (and thereby withstood) by the PTO. These are the result of the control actuations (Eq. 8). The controller-exerted force on the PTO can be described as a function of the commanded control force in the frequency domain as

$$F_{PTO}(\omega) = C(\omega)V(\omega) \quad (14)$$

To maximize the longevity of the PTO system, for instance to limit extreme loads resulting from large control responses in large waves, the exertions of the PTO can be considered by expanding Eq. 13

$$\eta_{opt} = \arg \min(W_1 P_{abs} + W_2 \sum |F_{PTO}|) \quad (15)$$

where W_1 and W_2 are positive 3-element vectors (one for each DOF) describing the relative weights of the objectives, and the vertical bars denote the amplitude of the spectra. This formulation penalizes both directions of PTO force equally.

F. Maximizing Device Fatigue Life

Secondly, deployment and maintenance of WECs can be a large component of device cost [30]. This implies that devices with long service lives may be more economical than more fragile devices, even if the latter may be more amenable to short-term power capture. Considering the deployment environment is an ocean wave field imparting consistent oscillatory loads, maximization of fatigue life will contribute to a longer service life. A convenient to formulation of fatigue damage accumulation in the frequency domain from [12] is

$$D_f = \frac{v_0^+ T}{K} (2\sqrt{2}\sigma_X)^m \Gamma\left(\frac{m}{2} + 1\right) \quad (16)$$

where v_0^+ is the mean zero-upcrossing rate

$$v_0^+ = \frac{1}{2\pi} \sqrt{\frac{m_2}{m_0}} \quad (17)$$

where T is the time (s) spent at the sea-state under consideration, K and m are parameters dictated by material selection and device geometry, the latter of which should not be confused with m_2 and m_0 , the spectral moments of the stress response spectrum. Finally, σ_X is the standard deviation of the Gaussian process, as estimated from the stress variance spectrum, and Γ denotes the Gamma function. This spectral formulation of fatigue damage is valid if the loading and the response

are assumed stationary random Gaussian processes, and the stress response can be further assumed to be narrow-banded. Ocean wave excitation is narrow banded [11], which implies that a PI controller reacting to this excitation will share a similar frequency range, so this is a reasonable assumption. Notably, since we rely upon linear transfer functions over the wave-excited frequency range, this approach will neglect any oscillations induced non-linearly. Furthermore, K and m are somewhat arbitrary constants in this context, as it is the relative fatigue damage of sets of control parameters under consideration herein. If a particular device-critical component has been selected for fatigue study, a specific selection can be advised by [31]. By similar arguments, T is also selected to be an arbitrary constant.

The force on the device PTO in each degree of freedom is considered with respect to fatigue load, although the approach could be applied to any device element subjected to cyclic loading if the appropriate transfer functions are identified. Based off of the linear system approach used throughout, the total force experienced by the device PTO will be the summation of the excitation force and controller actuations (Figure 1)

$$F_{TOT}(\omega) = F_a(\omega) + F_e(\omega) \quad (18)$$

where all variables are in the frequency domain. With this load as the Gaussian process under consideration, it follows that spectral moments can be described as

$$m_0 = \int_0^{2\pi} |F_{TOT}|^2 d\omega \quad (19)$$

and

$$m_2 = \int_0^{2\pi} \omega^2 |F_{TOT}|^2 d\omega \quad (20)$$

where the bounds of integration reflect the calculated domain of the impedance and excitation models used to calculate F_{TOT} (i.e., if we assume the spectral energy in contained in these bounds, then this is equivalent to the canonical bounds). Invoking Parseval's theorem ([32]), σ_X can be approximated as

$$\sigma_X = \sqrt{\frac{m_0}{L}} \quad (21)$$

where L is the length of the frequency vector. The fatigue damage accumulation can be added to the optimization cost function in a similar fashion, as

$$\eta_{opt} = \arg \min(W_1 P_{abs} + W_2 \sum (|F_{PTO}|) + W_3 D_f). \quad (22)$$

This formulation implies four unique useful control objective cases can be explored:

- 1) The maximization of power ($W_2 = W_3 = 0$)
- 2) The balancing of power and PTO load (i.e., $W_3 = 0$)
- 3) The balancing of power and fatigue damage ($W_2 = 0$)
- 4) The balancing of power, PTO load, and fatigue damage.

G. Adaptive Weights

As sea-states change in time, desired controller objective may also change. For example, in sufficiently small seas, power maximization may in fact be the sole objective, and load and fatigue damage mitigation may not be a concern. Stated mathematically, it is desirable that W_2 and W_3 can vary in time. A simple transition strategy is suggested in Eq. 23.

$$W_{j,k} = \{\Phi_{j,k} > p_{j,k}\} \alpha_{j,k} (\Phi_{j,k} - p_{j,k}) + \beta_{j,k} \int_{t_0,j,k}^t (\Phi_{j,k} - p_{j,k}) d\tau \quad (23)$$

where Φ is the value of the cost function argument ($\sum |F_{PTO}|$ or D_f), p is the user-specified threshold for j , the DOF (heave, surge, or pitch), and k , the objective (PTO load or fatigue damage), and the braces $\{\}$ indicate a logical check: the value of this term is a boolean 1 or 0. The threshold value for each objective likely would follow from a structural fatigue analysis of a particular area of concern on a specific device. The slope of these equations, α and β , must be carefully considered. Each spectral estimation is computed over a window and has an associated delay: a change in controller gain will only affect the cost function proportionally to how long it has been applied, up until the window fully populates with data related to the new gain selection. Thus the value of the cost function returned by the optimizer does not immediately reflect the “steady-state” performance of the selected gain, which may result in W continuing to increase even though the present selection of η would indicate optimal performance in a fully-populated window. The appropriate value of α and β depend on the window length and the local gradient of the cost function in the current sea-state. Generally, a steeply increasing weight value could lead to instability as a result of the windowing delay.

Adding an integral component to this calculation through a non-zero β will gradually increase relevant weighting over time as long as the threshold remains exceeded, and will provide a smoother transition to power-maximizing objectives when the operating condition goes below the threshold. The latter should allow for more aggressive adaptation gains which will speed adjustment time while avoiding the noted stability issues associated with the delay associated with spectral estimation. Here, t_0 is the first time a threshold is exceeded for a particular objective and degree of freedom. This adaptation weight has a lower saturation limit of 0, as negative weights are not meaningful in this context. With this saturation limit, anti-windup is needed on the integrator to maintain utility in the event that the operating condition falls below the specified threshold for an extended period [33] (Figure 6). This can also incorporate upper limits on weights. To this end, this is a simple implementation of a transition strategy: it is likely sub-optimal, but sufficient to demonstrate the concept.

III. RESULTS

A. Impedance Model

The impedance model identified from WEC-Sim simulation via Eq. 1 is shown alongside the impedance estimate as calculated strictly from BEM hydrodynamic coefficients (Eq. 3) in Figure 7. Although additional dynamic parameters were selected somewhat arbitrarily for the purposes of demonstration (Table I), they are not unreasonable for this device scale and geometry, thus emphasizing the potential importance of characterizing device impedance from experimental data. All forthcoming discussion will pertain to the former model of impedance Z_i , calculated from WEC-Sim simulation outputs using Eq. 1.

All “diagonal” impedance terms (i.e., input heave force to output heave velocity, input surge force to output surge velocity, etc.) show minor displacements of their resonant frequency and magnitude between the two estimates of Z_i , perhaps most significantly in pitch. Surge and heave show similar resonant periods at approximately 1.6 s, while pitch resonates at a shorter approximately 1.0 s period. The differences between BEM estimates of Z_i and that derived from data (Eq. 1) indicate the dynamic effects of the parameters included in the simulation that are not accounted for by the BEM estimate (Table I).

Coupling exists between surge and pitch degrees of freedom, shown in the lower half of Figure 7). These off-diagonal terms are more nearly identical between the BEM and simulation estimate. Further, the coupling terms are nearly symmetric, with surge-to-pitch showing a slightly larger magnitude for $\omega > 2$ rad/s.

B. Objective Surfaces

The performance of single objective, power maximizing control has been previously demonstrated [10]. This performance depends on the reliable convergence of the simple optimizer used to tune controller gains: this in turn depends on the convexity of the objective surface. For example, consider sea-state 10. The surfaces for each controller objective are shown for each DOF in Figures 8 through 10 as a function of controller gain selection. The colored contour indicates the power contour, with the brightest yellow indicating the maximum electrical power capture, with each contour line demarcating 10% decreases in power captures. PTO load contours and fatigue damage are superimposed with hashed and dotted contour lines, respectively. Because of the surge/pitch coupling, surge controller selection affects pitch DOF performance and vice-versa, implying that the coupled surge-pitch surface is in fact a four-dimensional domain comprised by proportional and integral gains in each surge and pitch. To facilitate visualization, a slice is taken at combinations of gains that result in optimum power capture, so that variations with respect to surge controller gains are presented on the plane defined by the pitch control gains that maximize power capture, and vice-versa. For surge and pitch, identical power surfaces are shown twice so that surge and pitch PTO loads and fatigue damage can be shown individually (Figures 9 and 10).

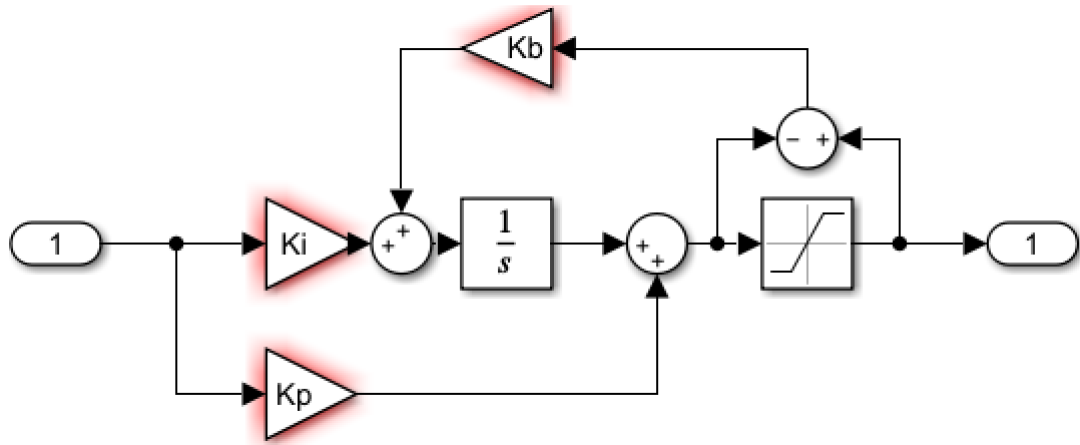


Fig. 6: Integral anti-windup employed in the weight adjustment implementation, proposed by [33]. For this implementation, the feedback gain K_b is equal to the integral weight adjustment gain K_i .

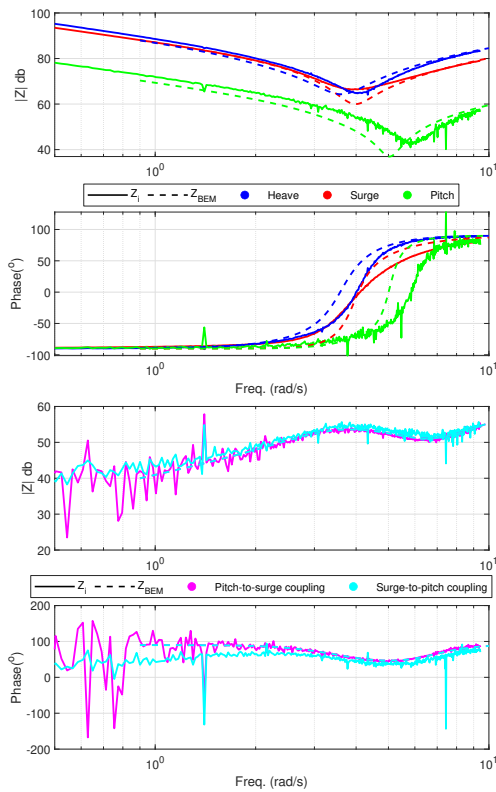


Fig. 7: The impedance model calculated from the as-deployed WEC-Sim simulation, compared to the impedance estimated from boundary element method for diagonal heave, surge, and pitch (top pair) and coupled off-diagonal surge and pitch (bottom pair).

Load contours are presented as a proportion of the respective load at the gain combination that maximizes power.

Notably for all degrees of freedom, diagonal (i.e., surge loads as functions of surge gains) contours show both fatigue damage and PTO load can be reduced by a minimum of 10% while retaining > 90% of maximum power capture, due to the relatively large range of gains associated with these high levels of power capture. This suggests that to at least a moderate extent, it is tenable to substantially reduce device loads of

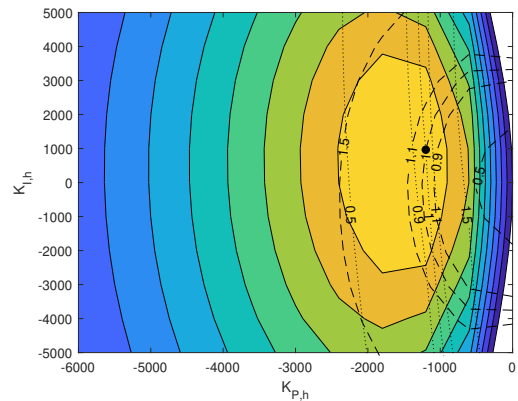


Fig. 8: Power contour of heave degree of freedom for Wave State 10. The hashed lines mark the PTO load contours and dotted lines are the fatigue damage contour for the heave DOF.

both investigated kinds without substantially reducing power. In the case of heave, both load contours are, in the vicinity of the power maximum, more nearly perpendicular, suggesting that some simultaneous mitigation of both load types may be attainable for heave in this sea-state (Figure 8). However, comparing the fatigue damage and PTO load contours for the diagonal surge and pitch cases, we see that they are anti-parallel, and mitigation of one kind of load through controller parameter adjustment will tend to exacerbate the other (Figure 9, top and Figure 10, bottom). This anti-parallel characteristic cannot also be said of the off-diagonal cases, however, the sensitivity of loading to control parameters of the other coupled DOF is limited, as indicated by the shallower contour lines (Figure 9, bottom and Figure 10, top).

The above observations do vary in extent with the selected sea-state, but remain generally true in the examined cases (others not shown). This suggests that the extent to which the individual objectives can be achieved, selections of weight values W that ensure a well-behaved surface, and, in turn, parameters used for adjusting weight values in Eq. 23, all are likely to vary with sea-state.

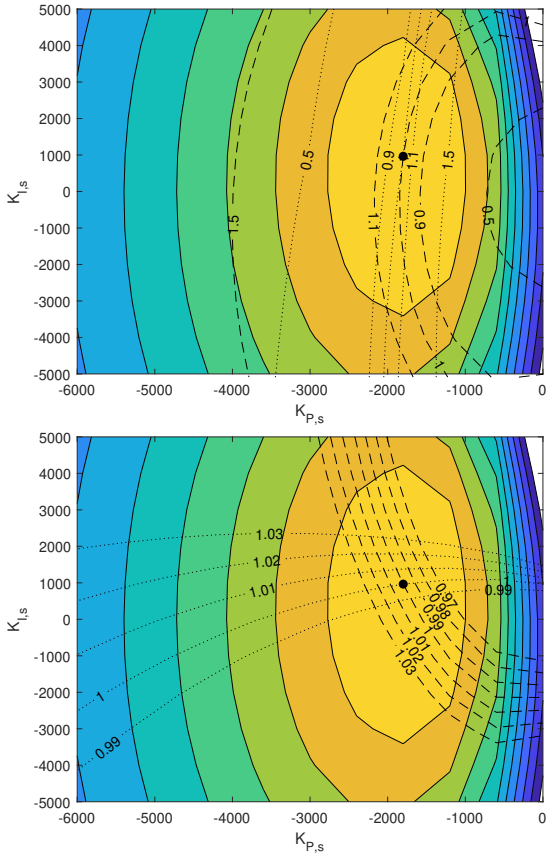


Fig. 9: Power contour of the coupled surge/pitch degree of freedom for Wave ID 10A. The contour slice is taken at the pitch gain that maximizes surge-pitch power capture, so that the presented axes show variation with surge gains. The hashed lines mark the PTO load contours and dotted lines are the fatigue damage contour for the surge DOF (top) and the pitch DOF (bottom).

C. Proof of Concept: Static Weights

Before exploring the more complicated case of transitioning control objectives by varying W in time, a simple proof-of-concept was demonstrated using static values of W given in Table III. The magnitude of the frequency domain estimate of $\sum |F_{PTO}|$ and D_f are shown along with controller gains over time for sea-state 10 (Figure 11).

As expected, non-zero static weights for W_2 and/or W_3 affects the optimal gain locations and relevant performance metrics. First, consider the simpler, uncoupled heave case. For Case 2 and 3, we see reductions in $\sum |F_{PTO}|$ and D_f relative to Case 1 respectively. Considering the excluded load, $\sum |F_{PTO}|$ is elevated relative to Case 1 for Case 3, and similarly, D_f is relatively elevated for Case 2. This highlights the somewhat contradictory nature of these load-mitigation objectives. However, as predicted by the region of perpendicular contours near the power maximum for heave in Figure 8, Case 4, which attempts to mitigate both sorts of loads, shows that both are in fact reduced relative to Case 1, though neither to the extent of Case 2 or 3.

Consideration of the coupled DOFs yields similar conclusions, with two notable distinctions. Firstly, as

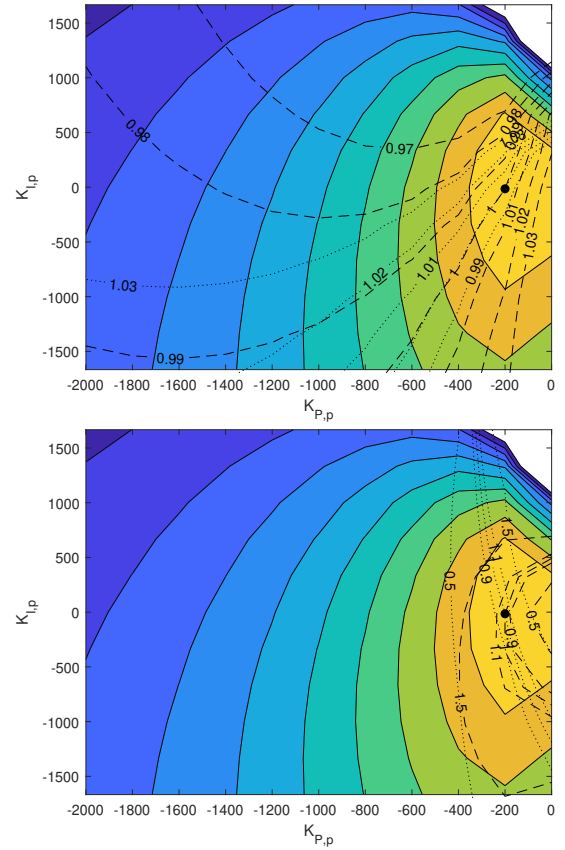


Fig. 10: Power contour of the coupled surge/pitch degree of freedom for Wave ID 10A. The contour slice is taken at the surge gain that maximizes surge-pitch power capture, so that the presented axes show variation with pitch gains. The hashed lines mark the PTO load contours and dotted lines are the fatigue damage contour for the surge DOF (top) and the pitch DOF (bottom).

predicted from the anti-parallel load contours in the diagonal surge surface (Figure 9, top), Case 4 does not simultaneously reduce $\sum |F_{PTO}|$ and D_f , instead acting similarly to Obj. 2, favoring a reduction in $\sum |F_{PTO}|$. For this DOF, the extent to which Obj. 4 favors Obj. 2 or 3 can be adjusted by changing W . Secondly, pitch shows substantial reductions in $\sum |F_{PTO}|$ and modest reductions in D_f for Obj. 2 through 4, with the magnitude of reductions for Obj. 4 being the most substantial. Comparing the tuned gains (Figure 11, top) to the diagonal pitch surface (Figure 10, bottom), this indicates that the controllers were operating in a region where the load contours are nearly orthogonal: this mutual reduction of load types is not unexpected in this region.

Controller coupling has a relatively smaller effect across DOFs, but it does affect the extent to which objectives can be achieved for coupled DOFs. For instance, the selection of pitch gains for Obj. 2 slightly increases surge $\sum |F_{PTO}|$ as a result of their coupling. This suggests that for some combinations of objectives and weights, the effects of coupling may create contradictions between objectives of coupled DOFs.

TABLE III: Weight matrix by case for Wave ID 10

Wave ID 10	Case 1			Case 2			Case 3			Case 4		
DOF	H	S	P	H	S	P	H	S	P	H	S	P
Power	25	25	25	25	25	25	25	25	25	25	25	25
PTO Load	0	0	0	0.1	0.2	0.2	0	0	0	0.1	0.2	0.2
Fatigue Damage	0	0	0	0	0	0	0.01	0.01	0.1	0.01	0.01	0.1

D. Adaptive Weights

The simulation of sea-state 10 was repeated with the weight adaption strategy described in Eq. 23, with the parameters in Table IV (Figure 12). The threshold values p were selected based upon the static runs to ensure that the relevant weight adjustment would take place for each control objective. In WEC-Sim simulation, a wave ramp of 20 s was used at the start of each run to ensure the solver is initially stable, however this wave ramp, and the delay associated with the windowing used to develop estimates of load spectra, ensure that thresholds are not exceeded immediately, and there is some initial time in which all control objectives appear identically. While an artifact of simulation approach here, this is analogous to a sea-state that increases in energy over time, and demonstrates the transition of weights in that context.

Generally, the adaptative controller weight mitigates the relevant load when the threshold is exceeded, and similar results to the static case are observed from then on. Notably, this threshold is regularly exceeded. In this way, the threshold p must be selected more conservatively than a hard constraint which can never be exceeded.

While the pitch DOF behaves as expected for reducing $\sum |F_{PTO}|$, it is not able to reliably mitigate D_f for Obj. 3 and 4. Because this was attained to some extent in the static case, this suggests that this combination of parameters in Eq. 23 leads to a combination of weights that, due to coupling with surge, limited performance in pitch to mitigate loads in surge: an example of a control objective conflict introduced due to coupling.

IV. DISCUSSION

A. Weight Selection

Some undesirable performance was observed in the pitch DOF of the adaptative weight case. Performance was also found to be susceptible to the parameters p , α , and β of Eq. 23. With certain exceptions, namely, the contradiction of two controls objectives, whether the contradiction is innate in a single DOF or arises through coupling, increasing the values of α and β decrease the amount by which p is exceeded. However, these values cannot be overly large, or else the delay associated with the spectral estimation procedure can lead to instability in weight selection, which can lead to the selection of unstable or otherwise intractable (e.g., through limitations on control hardware) gain selection. The extent to which control objectives contradict and appropriate weight selection for the static case also varies by sea-state. A study of $\sum |F_{PTO}|$ and D_f as a function of objective weight for four distinct Pierson-Moskowitz sea-states, outlined in Table V, is presented

in Figure 13. For Objective 4, both the weight values for Objective 2 and 3 were applied.

For all cases for which $W_2 > 0$, saturation in $\sum |F_{PTO}|$ is seen in while $W_2 > 0.5$, corresponding to zero controller gain. Similarly, D_f is seen to decrease monotonically for increasing W_3 . Although this does not readily saturate, controller gain values rapidly become intractably large. In this way, saturation limits on adaptive weight runs can be advised, either by saturation in $|F_{PTO}|$ or limitations on applicable gains.

Further, the extent of conflict between control objectives can be seen in Figure 13 by inspecting the trends in $\sum |F_{PTO}|$ and D_f for increasing W_2 or W_3 . For instance, for all sea-states in the pitch DOF, $\sum |F_{PTO}|$ decreases for increasing W_3 for a time before increasing rapidly. This implies that it is possible to simultaneously mitigate both kinds of load for this DOF, but only to a certain extent. A similar feature is observed in heave, but only for two of the investigated sea-states. While the magnitude of the concerned terms may vary with sea-state amplitude, these trends are consistent between sea-states of a common peak period.

A more systematic investigation to advise the optimal selection of α and β parameters, along with the ideal selection of the window length associated with frequency-domain calculation, is recommended as future work. It is specifically suggested to incorporate normalization factors in Eq. 22 such that all values of W are the same order of magnitude, as this may yield a more intuitive search space and remove some parameter sensitivity to wave height. Additionally, several estimations for device levelized cost-of-energy, the ultimate figure of merit, or proxies thereof exist and are conceivably formulated amenably for cost function incorporation [34].

B. Performance Considerations

The controller is capable of meeting multiple control objectives in a manner that adjusts both control parameters and the control objectives in response to changing sea-states, without relying on measurements of sea-state external to the device, and using only a single linear model of device impedance. The identification procedure for this model has been demonstrated here, and previously on physical systems [19] [35]. The simplicity and flexibility of this kind of controller thus has some desirable characteristics.

However, simultaneous mitigation of both investigated load types introduces complexities in the form of conflicting control objectives, both due to characteristics of individual DOFs or the coupling between them. Coupling was also seen to yield somewhat unintuitive performance for the mitigation of fatigue damage alone. More robust performance was seen for PTO load

TABLE IV: Parameters for weight adjustment (Eq. 23 by controller objective case)

Parameter DOF	Case 2			Case 3		
	H	S	P	H	S	P
p	1200	1200	150	8000	6000	375
α	1E-4	1E-4	1E-3	5E-7	5E-7	5E-4
β	5E-6	5E-8	5E-7	1E-7	5E-5	5E-7
Saturation limit	0.5	0.4	0.4	0.2	0.1	0.5
Wave ID	10					

TABLE V: Wave description for objective weight matrix study

Wave ID	H_s (m)	T_p
2A	0.127	1.6
7A	0.127	3.5
10A	0.254	3.5
13A	0.254	1.6

mitigation. While distinct sea-states do not confound these results, the performance of a set of adjustment parameters (Eq. 23) may not be optimal in all sea-states.

V. CONCLUSION

A 3-DOF point absorber that was previously tested in laboratory experiment was examined in simulation under a novel load-mitigating adaptive linear control law. First, the system identification procedure used in experiment was replicated for the simulation to develop a linear model of WEC intrinsic impedance. Next, this linear model was used to inform an optimization scheme which selects optimal proportional and integral control gains for each DOF. It was shown that PTO load and fatigue damage could generally be individually reduced to meaningful extents while retaining satisfactory power capture by adding these loads as penalty terms in the optimization cost function, though coupling between surge and pitch DOF were found to produce objective conflicts, and the load in surge or pitch may be increased in order to reduce this load in the other DOF. This can be affected by varying the objective weights in each DOF. Simultaneous mitigation of PTO load and fatigue damage was found to be possible in sea states and DOFs for which mutual reduction of these loads did not yield objective conflicts. Additionally, a transition strategy was demonstrated that adjusts objective function weights by comparing estimates of current loads to specified thresholds. While functional as presented, the optimization of this transition strategy, and a robust method of selecting appropriate parameters for a given device, is suggested as future work.

REFERENCES

- [1] J. Falnes, *Ocean Waves and Oscillating Systems*. Cambridge; New York: Cambridge University Press, 2002.
- [2] J. Hals, J. Falnes, and T. Moan, "A comparison of selected strategies for adaptive control of wave energy converters," *Journal of Offshore Mechanics and Arctic Engineering*, vol. 133, no. 3, p. 031101, March 2011. [Online]. Available: <http://offshoremechanics.asmedigitalcollection.asme.org/article.aspx?articleid=1456895>
- [3] G. Bacelli and R. G. Coe, "Comments on control of wave energy converters," *IEEE Transaction on Control System Technologies*, 2020.
- [4] J. Falnes, "A review of wave-energy extraction," *Marine Structures*, vol. 20, no. 4, pp. 185–201, Oct. 2007. [Online]. Available: <http://www.sciencedirect.com/science/article/pii/S0951833907000482>
- [5] O. Abdelkhalik, R. Robinett, G. Bacelli, R. Coe, D. Bull, D. Wilson, and U. Korde, "Control optimization of wave energy converters using a shape-based approach," in *ASME Power & Energy*, San Diego, CA, 2015.
- [6] A. Babarit, G. Duclos, and A. Clément, "Comparison of latching control strategies for a heaving wave energy device in random sea," *Applied Ocean Research*, vol. 26, no. 5, pp. 227–238, Jul. 2004. [Online]. Available: <http://www.sciencedirect.com/science/article/pii/S0141118705000209>
- [7] F. Fusco, J.-C. Gilloteaux, and J. Ringwood, "A study on prediction requirements in time-domain control of wave energy converters," in *Proceedings of the 8th IFAC Conference on Control Applications in Marine Systems*. Universitat Rostock, Germany: International Federation of Automatic Control, 2010.
- [8] R. G. Coe, G. Bacelli, V. Nevarez, H. Cho, and F. Wilches-Bernal, "A comparative study on wave prediction for WECs," Sandia National Laboratories, Tech. Rep. SAND2018-10945, 2018.
- [9] H.-N. Nguyen and P. Tona, "Continuously adaptive PI control of wave energy converters under irregular sea-state conditions," in *12th European Wave and Tidal Energy Conference (EWTEC)*, 2017.
- [10] D. D. Forbush, G. Bacelli, S. J. Spencer, and R. G. Coe, "A self-tuning wec controller for changing sea states," in *Proceedings of the 21st IFAC World Congress*, 2020.
- [11] R. G. Coe, G. Bacelli, and D. Forbush, "A practical approach to wave energy modeling and control," *Renewable and Sustainable Energy Reviews (submitted)*, 2020.
- [12] A. S. Zurkinden, S. H. Lambertsen, L. Damkilde, Z. Gao, and T. Moan, "Fatigue analysis of a wave energy converter taking into account different control strategies," in *ASME 2013 32nd International Conference on Ocean, Offshore and Arctic Engineering*. Citeseer, 2013, pp. V008T09A057–V008T09A057.
- [13] K. Ruehl, D. D. Forbush, Y.-H. Yu, and N. Tom, "Experimental and numerical comparisons of a dual-flap floating oscillating surge wave energy converter in regular waves," *Ocean Engineering*, vol. 196, p. 106575, 2020.
- [14] O. Abdelkhalik, R. Robinett, S. Zou, G. Bacelli, R. Coe, D. Bull, D. Wilson, and U. Korde, "On the control design of wave energy converters with wave prediction," *Journal of Ocean Engineering and Marine Energy*, vol. 2, no. 4, pp. 473–483, 2016. [Online]. Available: <http://dx.doi.org/10.1007/s40722-016-0048-4>
- [15] L. Ljung, *System identification - Theory for the User*. Prentice-Hall, 1999.
- [16] G. Bacelli and R. G. Coe, "WEC system identification and model validation," in *Marine Energy Technology Symposium (METS2017)*, Washington, D.C., 2017.
- [17] M. Folley, A. Babarit, B. Child, D. Forehand, L. O'Boyle, K. Silverthorne, J. Spinneken, V. Stratigaki, and P. Troch, "A review of numerical modelling of wave energy converter arrays," in *Proceedings of the 31st International Conference on Ocean, Offshore and Arctic Engineering*, Jul. 2012, pp. 535–545.
- [18] G. Bacelli, R. G. Coe, D. Patterson, and D. Wilson, "System identification of a heaving point absorber: Design of experiment and device modeling," *Energies*, vol. 10, no. 10, p. 472, 2017.
- [19] R. G. Coe, G. Bacelli, S. J. Spencer, D. Forbush, and K. Dullea, "Advanced WEC dynamics and controls MASK3 test," Sandia National Laboratories, Tech. Rep. SAND2019-15428, 2019.
- [20] R. G. Coe, G. Bacelli, S. J. Spencer, and H. Cho, "Initial results from wave tank test of closed-loop WEC control," Sandia National Laboratories, Albuquerque, NM, Tech. Rep. SAND2018-12858, 2018.
- [21] K. Ruehl, D. Ogden, Y.-H. Yu, A. Keester, N. Tom, D. Forbush, and J. Leon, "Wec-sim v4.4," October 2021. [Online]. Available: <https://zenodo.org/badge/latestdoi/20451353>
- [22] K. Hasselmann, T. Barnett, E. Bouws, H. Carlson, D. Cartwright, K. Enke, J. Ewing, H. Gienapp, D. Hasselmann, P. Kruse-

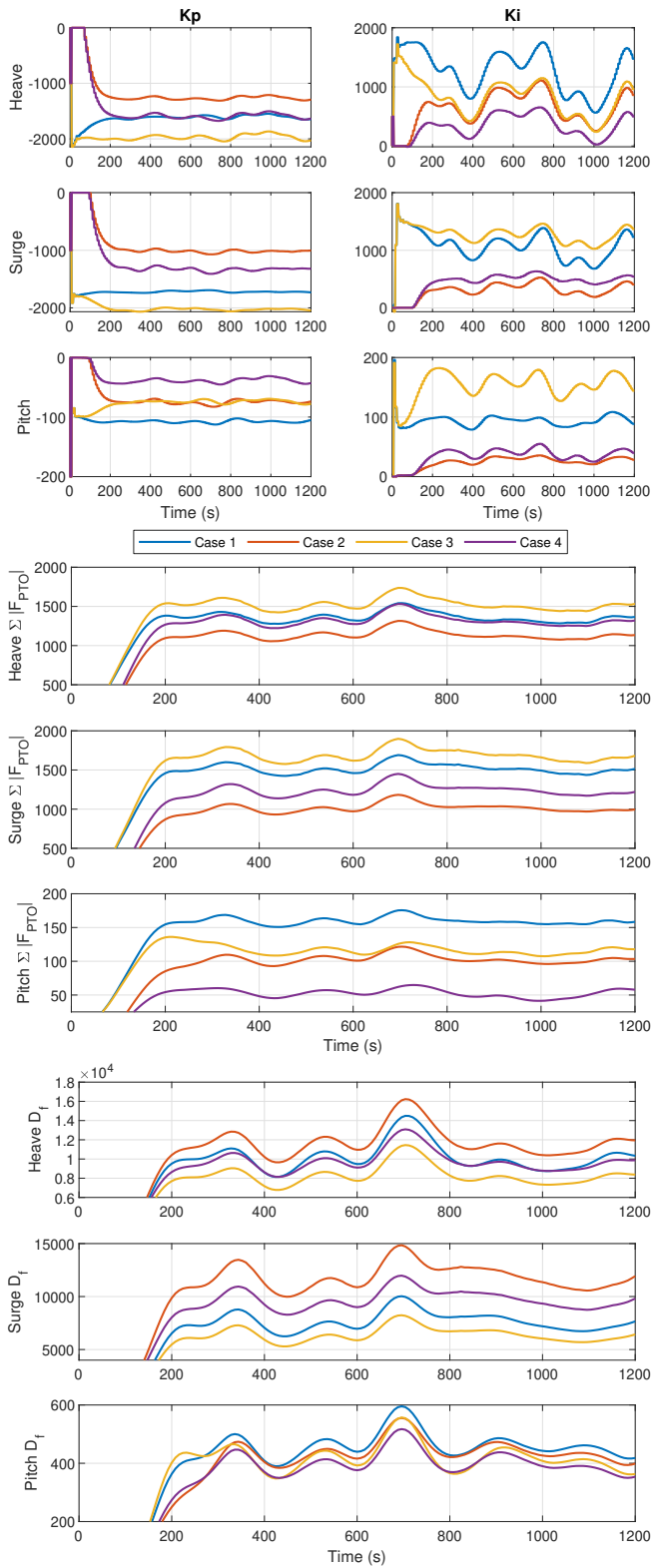


Fig. 11: Controller gains (top), $\sum |F_{PTO}|$ (middle), F_{TOT} (bottom) over time (s) for heave, surge, and pitch for the static weight case. The legend given on the middle figure is used throughout, with the color denoting controls objectives, and the line style indicating weight adaptation approaches.

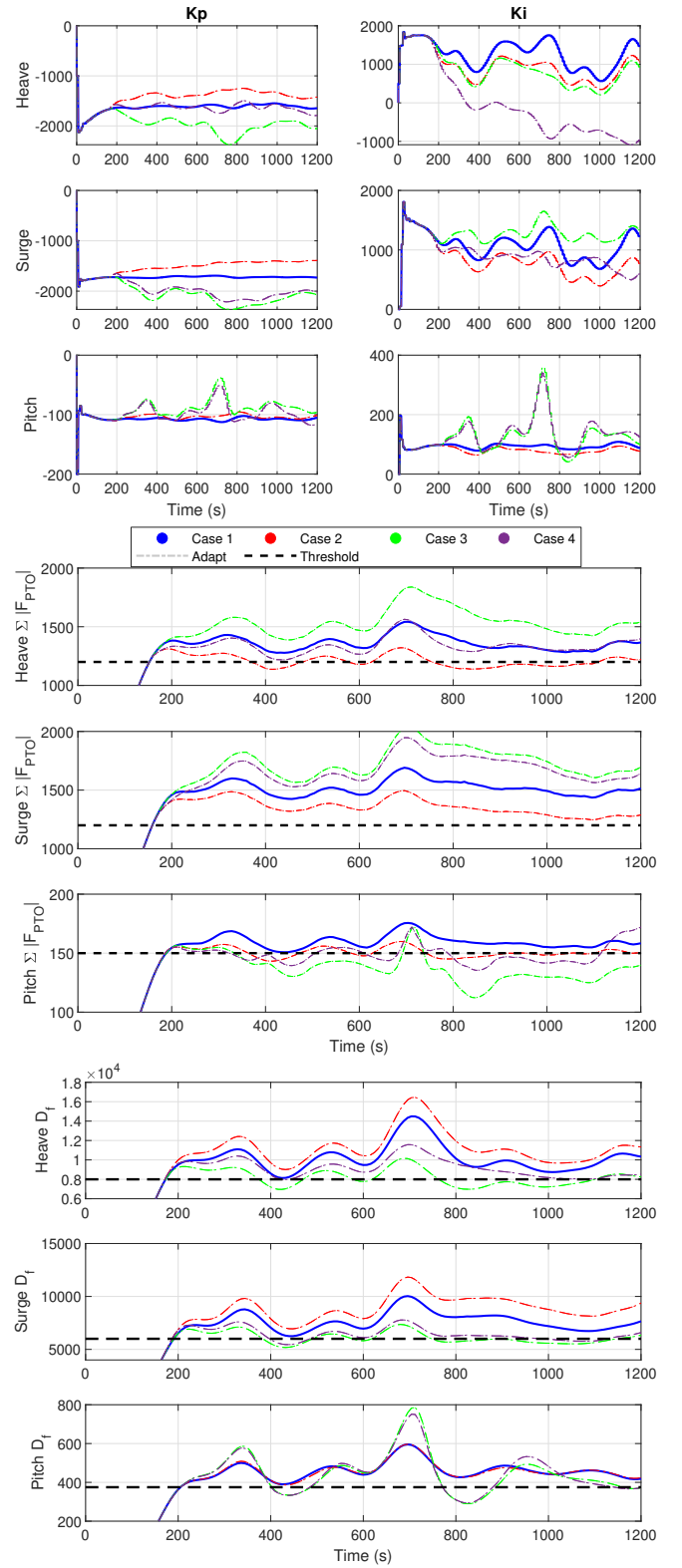


Fig. 12: Controller gains (top), $\sum |F_{PTO}|$ (middle), F_{TOT} (bottom) over time (s) for heave, surge, and pitch. The legend given on the middle figure is used throughout, with the color denoting controls objectives, and the line style indicating weight adaptation approaches. The horizontal black dashed line indicates the threshold (Eq. 23) for each objective and degree of freedom.

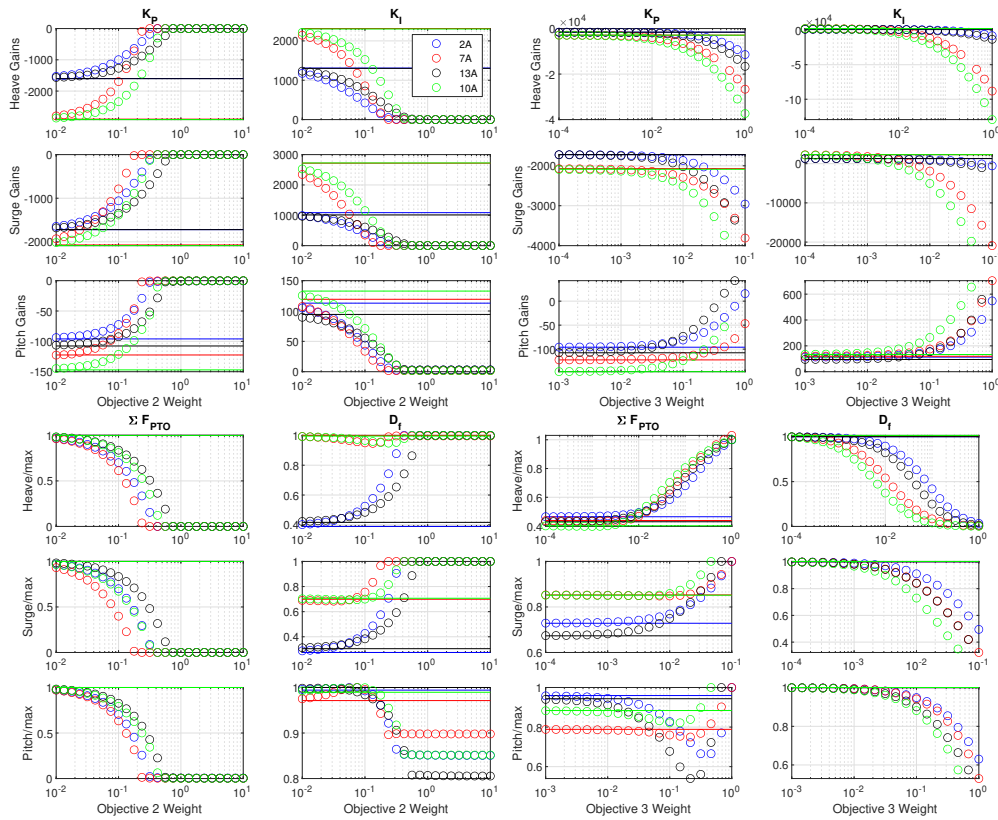


Fig. 13: Controller gains (top row) and $\sum |F_{PTO}|$ and D_f (bottom row) as a function of W_2 (left column) and W_3 (right column) for heave, surge, and pitch. To facilitate visualization for all sea states, the bottom row is normalized. The solid line indicates the plotted value at a weight value of zero, for comparison. For this study, $W_3 = 0$ when $W_2 > 0$, and vice versa.

- man *et al.*, "Measurements of wind-wave growth and swell decay during the joint north sea wave project (JONSWAP)," *Ergänzungsheft 8-12*, 1973.
- [23] J. Falnes, "Optimum control of oscillation of wave-energy converters," *International Journal of Offshore and Polar Engineering*, vol. 12, no. 02, pp. 147–155, 2002.
- [24] O. Kimmoun, H. Branger, and C. Kharif, "On short-crested waves: experimental and analytical investigations," *European Journal of Mechanicals - B/Fluids*, vol. 18, no. 5, pp. 889–930, Sep. 1999.
- [25] G. Bacelli, S. J. Spencer, D. C. Patterson, and R. G. Coe, "Wave tank and bench-top control testing of a wave energy converter," *Applied Ocean Research*, vol. 86, pp. 351 – 366, 2019.
- [26] H. Cho, G. Bacelli, and R. G. Coe, "Model predictive control tuning by inverse matching for a wave energy converter," *Energies*, vol. 12, no. 21, p. 4158, Oct 2019. [Online]. Available: <http://dx.doi.org/10.3390/en12214158>
- [27] V. Nevarez, G. Bacelli, R. G. Coe, and D. G. Wilson, "Feedback resonating control for a wave energy converter," in *Proceedings of SPEEDAM2018*, 2018.
- [28] O. Abdelkhalik, S. Zou, G. Bacelli, R. D. Robinett, D. G. Wilson, and R. G. Coe, "Estimation of excitation force on wave energy converters using pressure measurements for feedback control," in *OCEANS 2016 MTS/IEEE Monterey*, Sept 2016, pp. 1–6.
- [29] R. G. Coe and V. S. Neary, "Review of methods for modeling wave energy converter survival in extreme sea states," in *Marine Energy Technology Symposium (METS)*, Seattle, WA, 2014.
- [30] V. S. Neary, M. Lawson, M. Previsic, A. Copping, K. C. Hallett, A. LaBonte, J. Rieks, and D. Murray, "Methodology for design and economic analysis of marine energy conversion (mec) technologies." Sandia National Laboratories, Tech. Rep. SAND2014-9040, 2014.
- [31] Anon, "Modelling and analysis of marine operations," DNV, Tech. Rep. DNV-RP-H103, 2011.
- [32] W. Kaplan, *Advanced Calculus*. Addison Wesley, 1991.
- [33] K. Aström and R. Murray, *Feedback Systems: An Introduction for Scientists and Engineers*. Princeton University Press, 2010.
- [34] A. De Andres, E. Medina-Lopez, D. Crooks, O. Roberts, and H. Jeffrey, "On the reversed lcoe calculation: Design constraints for wave energy commercialization," *International journal of marine energy*, vol. 18, pp. 88–108, 2017.
- [35] R. G. Coe, G. Bacelli, D. Forbush, S. J. Spencer, K. Dullea, B. Bosma, and P. Lomonaco, "Foswec dynamics and controls test report," Sandia National Laboratories, Tech. Rep. SAND2020-11695, 2020.